Anticancer potential of silver nanoparticles biosynthesized using Catharanthus roseus leaves extract on cervical (HeLa229) cancer cell line

Article *in* Scientific African · May 2024

DOI: 10.1016/j.sciaf.2024.e02268

4 authors, including:

Hadil Hussein
Jomo Kenyatta University of Agriculture and Technology
3 PUBLICATIONS **1** CITATION
SEE PROFILE

Esther Maina
University of Nairobi
43 PUBLICATIONS **1,573** CITATIONS
SEE PROFILE

Scientific African 25 (2024) e02268

Contents lists available at ScienceDirect

Scientific African

journal homepage: www.elsevier.com/locate/sciaf

Anticancer potential of silver nanoparticles biosynthesized using *Catharanthus roseus* leaves extract on cervical (HeLa229) cancer cell line

Hadil S. Hussein [a,*], Caroline Ngugi [b], Festus M. Tolo [c], Esther N. Maina [d]

[a] *Department of Molecular Biology and Biotechnology. Pan African University Institute for basic sciences, technology and Innovation (PAUSTI), P. O. Box 62000-00200, Nairobi, Kenya*
[b] *Department of Medical Microbiology, Jomo Kenyatta University of Agriculture and Technology (JKUAT), P. O. Box 62000-00200, Nairobi, Kenya*
[c] *Centre for Traditional Medicine and Drug Research (CTMDR), Kenya Medical Research Institute, PO Box 54840, 00200 Nairobi, Kenya*
[d] *Department of Biochemistry, Faculty of Science and Technology, University of Nairobi(UON). P. O. Box 30197-00100, Nairobi, Kenya*

ARTICLE INFO

Editor: DR B Gyampoh

Keywords:
Silver nanoparticles
Characterization
Cytotoxicity
Antimetastatic activity
Gene expression analysis

ABSTRACT

Cervical cancer is a significant global health issue among women due to its prevalence and impact on morbidity and mortality, especially in low- and middle-income countries. This underscores the critical necessity for the development of anticancer treatments that are not only more efficient but also safer. This study introduces a novel approach to combating cervical cancer by synthesizing silver nanoparticles (AgNPs) using aqueous *Catharanthus roseus* leaves extract and evaluating their anticancer activity. The aqueous extract of *C. roseus* showed remarkable potential to reduce silver ions rapidly. UV–Vis spectroscopy confirmed the formation of AgNPs, with a characteristic surface plasmon resonance (SPR) band observed at 429 nm. TEM/EDX and FE-SEM analysis confirmed the presence of spherical AgNPs with uniform size distribution. XRD analysis confirmed the face-centered cubic (FCC) structure of metallic silver in AgNPs. Moreover, AgNPs exhibited significant antiproliferative and cytotoxic effects on HeLa229 cells, with higher selectivity towards cancer cells compared to normal cells. Moreover, wound healing assays showed the robust antimetastatic potential of AgNPs by inhibiting cancer cell migration. The real-time reverse transcription polymerase chain reaction analysis demonstrated the impact of AgNPs on inducing apoptosis and cell cycle arrest. Overall, these findings highlight the promising role of AgNPs synthesized from *C. roseus* extract as effective anticancer agents,offering a promising alternative to conventional chemotherapy with potentially reduced side effects and increased efficacy.

Introduction

Globally, cancer is a significant public health burden; in 2020, there were 19.3 million new cancer cases and 10.3 million deaths from cancer, which are predicted to rise to 28.4 million by 2040 [1]. According to a study published in 2021, cervical cancer is the fourth most common cause of cancer death among women after breast, colorectal, and lung cancers, with an estimated 604,000 new cases and 342,000 deaths in 2020 [2]. Approximately 85 % of female malignancies occur in low- and middle-income areas; it accounts for over 12 % of all malignancies [3]. Conventional cancer treatments like chemotherapy, radiation therapy, targeted therapy, and

* Corresponding author.
E-mail address: Hussein.hadil@students.jkuat.ac.ke (H.S. Hussein).

https://doi.org/10.1016/j.sciaf.2024.e02268
Received 7 February 2024; Received in revised form 17 May 2024; Accepted 27 May 2024
Available online 28 May 2024

immunotherapy have problems that make them hard to use effectively [4,5]. Therefore, advanced cancer research must discover alternative formulations for addressing these shortcomings [6].

Nanoparticles have distinctive physical and chemical characteristics, including their small size (between 1 and 100 nm), optical activity, chemical reactivity, high mechanical strength, and large surface area [7,8]. The broad range of applications for nanoscale materials, particularly in biomedical fields, is drawing increased attention to their use [9]. There are several types of metal nanoparticles, including gold, silver, titanium, zinc oxide, and others. Among those nanoparticles, silver nanoparticles (AgNPs) find extensive application in the biomedical field, serving various purposes such as anti-inflammatory, antioxidant, antimicrobial, antibacterial, and anticancer activities [10,11]. Silver nanoparticles can be synthesized using chemical, physical, and biological methods. Among these, the biological approach, specifically utilizing plant extracts, stands out for its eco-friendly, safe, and cost-effective characteristics in contrast to chemical and physical methods [12,13]. Notably, this approach eliminates the necessity for specialized conditions such as high temperatures, power, carcinogenic solvents, expensive reagents, or high-pressure conditions often required in chemical and physical methods [14,15].

Catharanthus roseus belongs to the Apocynaceae family, originating from the Indian Ocean island of Madagascar, and this plant has been identified as a source of diverse indole alkaloids known for their anticancer properties [16,17]. The efficacy of herbal remedies is closely tied to bioactive compounds inside the extract, such as flavonoids, tannins, and terpenoids. These compounds contribute to the pharmacological activities of herbal remedies. Nevertheless, despite their ability to dissolve in water, these compounds are difficult to absorb due to their limited capacity to pass through lipid membranes easily. Their significant molecular sizes and restricted absorption decrease bioavailability, ultimately affecting their effectiveness [18]. According to certain studies, herbal remedies have a good effect in tests in vitro but poor activity in investigations in vivo [19]. Researchers have combined herbal medicine and nanotechnology to ensure maximum patient compliance and avoid repetitive administration to create novel delivery systems for natural compounds. These systems increase therapeutic value by increasing bioavailability and lessening the need for recurrent administration to counteract noncompliance [20].

In this study, we present a novel approach to cervical cancer therapy by investigating the potential anticancer properties of silver nanoparticles (AgNPs) synthesized using aqueous *Catharanthus roseus* leaves extract against on cervical cancer (HeLa 229) cell lines. To our knowledge, this is the first documented exploration of the specific impact of AgNPs derived from *C. roseus* extract on cervical cancer. Additionally, we delve into the molecular mechanisms underlying the effect of AgNPs on cervical cancer cells, providing unprecedented insights into their therapeutic potential, and representing a significant advancement in the field of cervical cancer therapy with eco-friendly synthesis methods.

Materials and methods

Plant materials

C. roseus leaves were obtained from Kiambu County, Kenya, and the plant's authenticity was verified at Jomo Kenyata University of Agriculture and Technology Botanical Herbarium (JKUATBH) by Mr. Muchuku Kamau, assigned reference number HSH-JKUATBH/001/2023.

Preparation of the plant extract

C. roseus leaves were cleaned with distilled water and dried naturally under shade. After completely drying leaves, they were carefully milled into a powder. In a water bath, 50 g of powdered leaves were dissolved in 1 liter of distilled water, and the mixture was incubated at 60°C for one hour, followed by gradual cooling at room temperature. Subsequent to this process, the solution underwent filtration utilizing Whatman filter paper No. 1 (Whatman International Ltd., Maidstone, England). The resulting filtrate was carefully preserved at −4°C to facilitate its utilization in the synthesis of AgNPs [21].

Qualitative phytochemical screening

C. roseus leaves extract was tested for phytochemicals such as flavonoid, tannin, and phenol using the ferric chloride test. At the same time, alkaloids were detected using the Mayers test, saponin (Froth test), glycoside (NaOH test), and terpenoid (Salkowski's test) by previously published protocols [22].

Synthesis of silver nanoparticles

In a 100 ml Erlenmeyer flask, 10 ml of *C. roseus* aqueous extract was mixed with 90 ml silver nitrate (1 mM). The mixture was then heated at 60°C and stirred continuously for 24 h with a magnetic stirrer [23]. Afterward, the solution containing AgNPs was centrifuged at a speed of 10,000 rpm for 20 min. The obtained pellet underwent three washings with double distilled water to eliminate contaminants, followed by lyophilization for 72 h in a freezer-dryer apparatus.

Characterization of silver nanoparticles

Visual color change

The visual color change during the synthesis of AgNPs was monitored as an indicator of the reduction of silver ions [24]. Silver nitrate was used as a negative control.

UV–Vis spectroscopy

The production of AgNPs from the aqueous extract of *C. roseus* was verified using a UV-1800 UV/VIS spectrophotometer (Shimadzu, Kyoto, Japan). Both the aqueous extract and silver nitrate were employed as blanks to establish baseline readings and identify the distinctive absorption peaks associated with forming AgNPs.

Fourier-transform infrared spectroscopy analysis (FT-IR)

The functional groups on the AgNPs' surface are determined using FT-IR analysis. The AgNPs were ground with Potassium bromide (KBr) pellets and analyzed in an FT-IR-8000 spectrophotometer model (Shimadzu, Kyoto, Japan) in the range of 500–4000 cm^{-1} [25].

Field emission scanning electron microscopy analysis (FE-SEM)

The shape and size of AgNPs were examined using FE-SEM. Samples were drop-deposited, air-dried, and sputter-coated with gold for high-resolution imaging. And images were subsequently recorded.

Transmission electron microscope and energy-dispersive X-ray spectroscopy (TEM/EDX)

The surface shape and size of the AgNPs were examined using TEM with a voltage of 150 kV. A copper grid held the silver nanoparticles, and TEM images were taken at various magnifications. A further analysis of the silver nanoparticles' elemental composition was performed using EDX [26].

X-ray- diffraction analysis (XRD)

X-ray Diffraction (XRD) with Cu Kα radiation in the -2θ configuration to assess the crystallinity and the average crystalline size of the AgNPs [27].

Optimization of biosynthesis of AgNPs

The optimization of synthesis parameters, including incubation time, pH, and plant extract concentration, was carried out to achieve rapid and maximum production of AgNPs. The impact of pH values, ranging from 3, 5, 7, 9, to 11, was examined. Reaction time was meticulously monitored 6 hours to determine the optimal conditions for AgNPs production. The aqueous extract concentration was further diluted in a (1 mM) $AgNO_3$ solution to determine the optimal concentraction of the plant. The absorbance of silver nanoparticles was quantified using UV–VIS spectroscopy. These optimization steps aimed to enhance the efficiency and yield of AgNPs synthesis [28].

Stability study

The stability of AgNPs was investigated by varying pH, temperature, and storage conditions. Different pH levels (2, 4, 7, 9, and 11) were tested to assess their impact on AgNPs. Heat stability was evaluated by subjecting the reaction mixture to 37, 50,70, 90, and 100 °C for 30 min. Storage stability testing kept the synthesized AgNPs for four months at 37, 4, −20, −40, and −80 °C and monitored using UV–Vis spectroscopy [29].

Cell culture

The Vero CCL-81 and HeLa 229 cell lines were cultured in Minimum Essential Medium (MEM) supplemented with 10 % Fetal Bovine Serum (FBS) (Sigma, Missouri, Germany). The medium was supplemented with L-glutamine and 1 % penicillin-streptomycin (Beijing Solarbio Science and Technology Co., Ltd., China). The cell cultures were kept at 37 °C in a controlled environment with 5 % CO2 and 95 % air in an incubator.

Antiproliferative and cytotoxicity(resazurin) assay

In 96-well plates, Vero CCL-81 and HeLa229 cell lines were seeded at 1×10^3 cells/well. Then, they were treated with treatment for 24 and 48 h using various concentrations (200, 100, 50, 25, 12.25, and 6.25 μg/ml) of the aqueous extract and AgNPs. After the treatment, a volume of 20 μl of resazurin solution was added and incubated for 4 hours. A microplate reader (Multiskan GO Microplate Reader, Massachusetts, USA) was used to measure fluorescence. The negative control received only 0.2 % DMSO, while the positive control underwent treatment with vincristine sulfate (standard reference drug). The cell viability percentage was determined by analyzing optical density measurements, enabling the calculation of IC_{50}, C_{50}, and Selectivity Index (SI).

Data was analyzed as follows for both the Vero-81 and HeLa229 cell lines to determine the cell viability percentage:

% Cell viability will be calculated using the following formula [30];

$$\% \text{ Cell viability } = \frac{Control\ OD\ --Sample\ OD}{Control\ OD}\ x\ 100$$

Where:
OD = optical density

Wound healing assay

The HeLa229 cells were placed in 24-well plates at 1×10^5 cells per well to create monolayers. These monolayers were then incubated in MEM media overnight. To make linear incisions, 200 μl pipette tips were utilized. After being washed with PBS to eliminate cell debris, wounded monolayers were treated with AgNPs and the aqueous extract at IC_{50} concentration. The wound gaps were imaged using EVOS microscopy at regular intervals (0, 24, 48, and 72 h). The area of cell-free wounds was then computed using the ImageJ program (ImageJ, Maryland, USA) [31].

Quantitative real-time polymerase chain reaction (RT-qPCR)

The study utilized RT-qPCR to examine the molecular impacts of AgNPs and the aqueous extract on HeLa229 cells. The cells were subjected to RNA extraction using an RNA extraction kit (Beijing Solarbio Science and Technology Co., Ltd., Beijing, China). Subsequently, complementary DNA (cDNA) was synthesized using the SensiFASTTM cDNA Synthesis Kit (Meridian Bioscience Inc., Ohio, USA). The quantification of gene expression levels related to apoptosis and cell cycle genes was performed using Luna Universal qPCR Master Mix (New England Biolabs, Massachusetts, USA). The ΔΔCt method was used to determine the relative gene expression levels. The primer sequences obtained from Macrogen Europe BV are provided in Table 1.

Statistical analysis

The statistical analysis were performed using Origin Pro-software and GraphPad Prism version 9 (GraphPad Software Inc., San Diego, CA, USA). The data presentation employed the mean ± standard error of the mean (SEM). One-way analysis of variance (ANOVA) was applied for comprehensive data analysis, and multiple comparisons were assessed using Tukey's post hoc test. The statistical significance was established at a threshold of $P < 0.05$.

Results and discussion

Qualitative phytochemical screening

C. roseus leaves aqueous extract revealed the presence of various chemical compounds, including terpenoids, Saponins, alkaloids, phenols, flavonoids, and tannins, except the glycosides, as outlined in Table 2, in disagree with the findings of [32]. The colorimetric method was employed for the qualitative analysis, utilizing color change indicators to detect the presence of specific compounds upon adding reagents [33]. Notably, flavonoids, characterized by hydroxyl groups (-OH), were identified. These hydroxyl groups, which carry a negative charge, can bind to the Ag+ surface and facilitate ion reduction [34]. Furthermore, it is recognized that phenolic compounds and flavonoids are involved in the reduction reaction [35]. Terpenoids and tannins can contribute electrons to convert Ag^+ ions to Ag^0 [36]. Therefore, Alkaloids, phenols, flavonoids, tannins, terpenoids, and saponins are among the substances in the *C. roseus* aqueous extract that are highly likely to be involved in the biosynthesis of AgNPs (Supplementary Figure S1).

Visual change and UV–Vis spectroscopy

The aqueous extract of *C. roseus* reduced silver ions to form the AgNPs. The reaction mixture (*C. roseus* extract + $AgNO_3$) had a pale

Table 1
List of primers sequence.

Gene name	Sequence
p53	Forward- CTTCGAGATGTTCCGAGAGC
	Reverse- GACCATGAAGGCAGGATGAG
Caspase 9	Forward- CCTGCCCGCTGTTTGGA
	Reverse- GCTGGGAAATGGGGAGACAA
CDK1	Forward- GAACACCACTTGTCCCTCTAAGAT
	Reverse- CTGCTTAGTTCAGAGAAAAGTGC
Beta Actin	Forward- GCCAACTTGTCCTTACCCAGA
	Reverse- AGGAACAGAGACCTGACCCC
p21	Forward- GCGACTGTGATGCGCTAATG
	Reverse- TTAGAAGCTTGGCAAAGGGC
BcL-2	Forward- GGCCTCAGGGAACAGAATGAT
	Reverse- TCCTGTTGCTTTCGTTTCTTTC

Table 2
Phytochemical screening result of *C. roseus* leaves aqueous extract.

S/N	Phytoconstituents	Test performed	Aqueous extract
1	**Alkaloid**	**Mayer's Test**	+
2	**Saponins**	**Foam test**	+
3	**Terpenoids**	**Salkowski test**	+
4	**Flavonoids**	**Ferric Chloride Test**	+
5	**Tannins**	**Ferric Chloride Test**	+
6	**Phenols**	**Ferric Chloride Test**	+
7	**glycosides**	**NaOH solution**	–

(+) = present and (-) =absent.

yellow color at first, but after 12 hours, it turned reddish brown; this confirms the production of silver nanoparticles, as shown in Fig. 1 (a).

The reduction of metallic ions (Ag^0) from silver ions (Ag^+) is indicated by the surface plasmon resonance (SPR) band, which is centered at 429 nm in the UV–Vis spectra of AgNPs, as shown in Fig. 1(b). The synthesis of AgNPs has been reported in various studies, each revealing distinct UV/VIS absorption maxima. Mukunthan et al. (2011) observed absorption maxima at 440 nm [37], while Ponarulselvam et al. (2012) reported a distinct absorption peak at 410 nm [38]. Moreover, the observed broadening of the band supports the polydisperse nature of AgNPs.

FT-IR analysis

The functional groups on the AgNP's surface can be identified through FTIR spectroscopy. In the present study, FTIR spectra were utilized to determine the phytochemicals present in *C. roseus* leaves extract that are responsible for the reduction reaction, as shown in Fig. 2. The FTIR analysis of *C. roseus* leaves aqueous extract revealed two medium peaks at 3016 cm^{-1} and 2972 cm^{-1}, which shifted to 3030 cm^{-1} and 2968 cm^{-1}, respectively, in AgNPs. These shifts were attributed to the C—H stretch of alkene and the C—H stretch of alkane, respectively. Additionally, weak bands observed at 2939 cm^{-1} in the aqueous extract changed to 2972 cm^{-1} in AgNPs, corresponding to the O—H stretch in alcohol. Furthermore, the aqueous extract exhibited a medium peak at 1570 cm^{-1} associated with N—H stretch in amine, which shifted to 1631 cm^{-1} in AgNPs. Another medium band at 1438 cm^{-1}, present in both the aqueous extract and AgNPs, was attributed to the O—C stretch in carboxylic acid. Five strong bands at 1525 cm^{-1}, 1367 cm^{-1}, 1220 cm^{-1}, 1066 cm^{-1}, and 526 cm^{-1} were observed, corresponding to nitro compound, Sulfonate, Vinyl ester, Primary alcohol, and Halo-compound, respectively, in both the aqueous extract and AgNPs. Different functional groups, including alkene, alkane, carboxyl, alcohol, esters, nitro compound, sulfonate, vinyl ester, primary alcohol, and halo-compound groups, were confirmed to be present in the aqueous extract of *C. roseus* leaves by the FT-IR analysis. Notably, the medium band at 1631 cm^{-1} can be attributed to N—H, probably to the presence of amines, which may be responsible for reducing Ag^{+1} to AgNPs [39].

TEM/EDX analysis

The AgNPs size ranged from 6 to 33 nm, displaying predominantly spherical forms and exhibiting uniformity [40], as shown in Fig. 3(a,b). Through analysis of Selected Area Electron Diffraction (SAED) patterns, images showed ring patterns with light spots on a dark field, revealing the crystalline structure of the silver nanoparticles, as shown in Fig. 3(c). The EDX spectra revealed a prominent peak at approximately 3 keV, confirming the presence of elemental silver [41]. Furthermore, copper signals corresponding to the

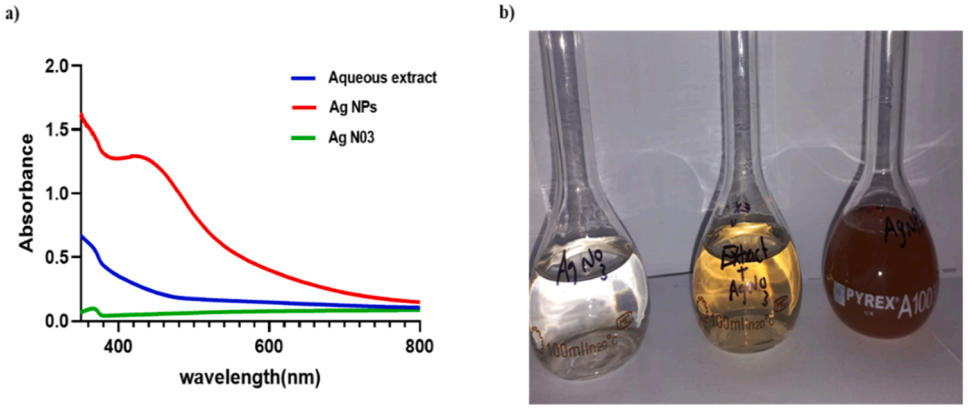

Fig. 1. (a) UV–Vis spectra of synthesized AgNPs of *C. roseus* leaves aqueous extract at 24 h of incubation, values expressed as mean ± SE of the mean (n = 3), (b) Photo showing the color of synthesized AgNPs.

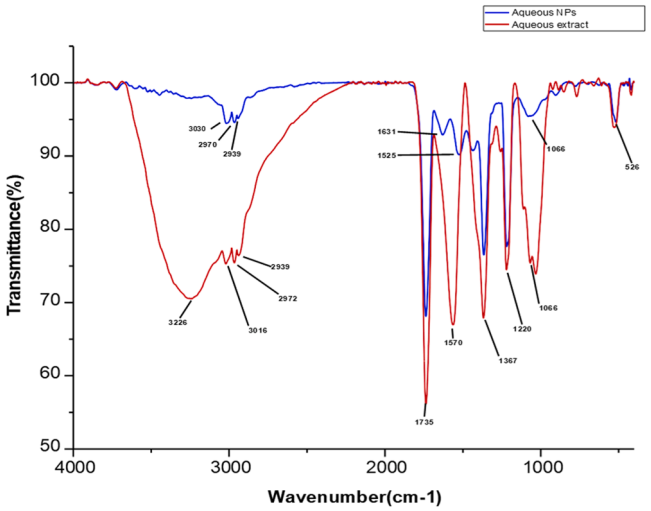

Fig. 2. FT-IR spectra of the functional groups of the AgNPs and *C. roseus* leaves aqueous extract.

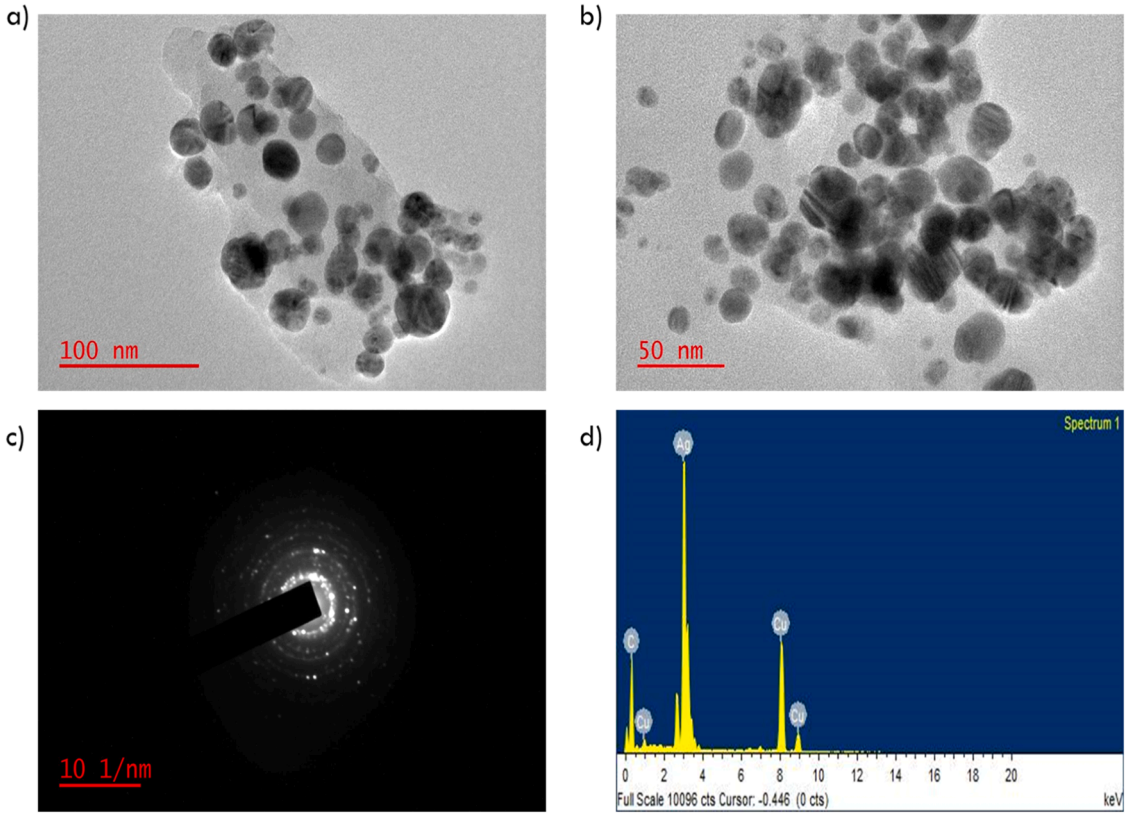

Fig. 3. TEM images of AgNPs at magnifications of (a) 100 nm and (d) 50 nm. (c) SAED and (d) EDX, a spectrum of AgNPs.

study's TEM grid were seen in the EDX spectrum Fig. 3(d).

FE-SEM analysis

FE-SEM images showed that the AgNPs with diameters between 12 and 31 nm were uniform and spherical, as shown in Fig. 4(a,b) and Table (3). The findings are consistent with previous reports in the literature [42,43]. This variation in size could result from the complex interactions between these compounds and the silver ions during the synthesis process. Notably, the absence of apparent

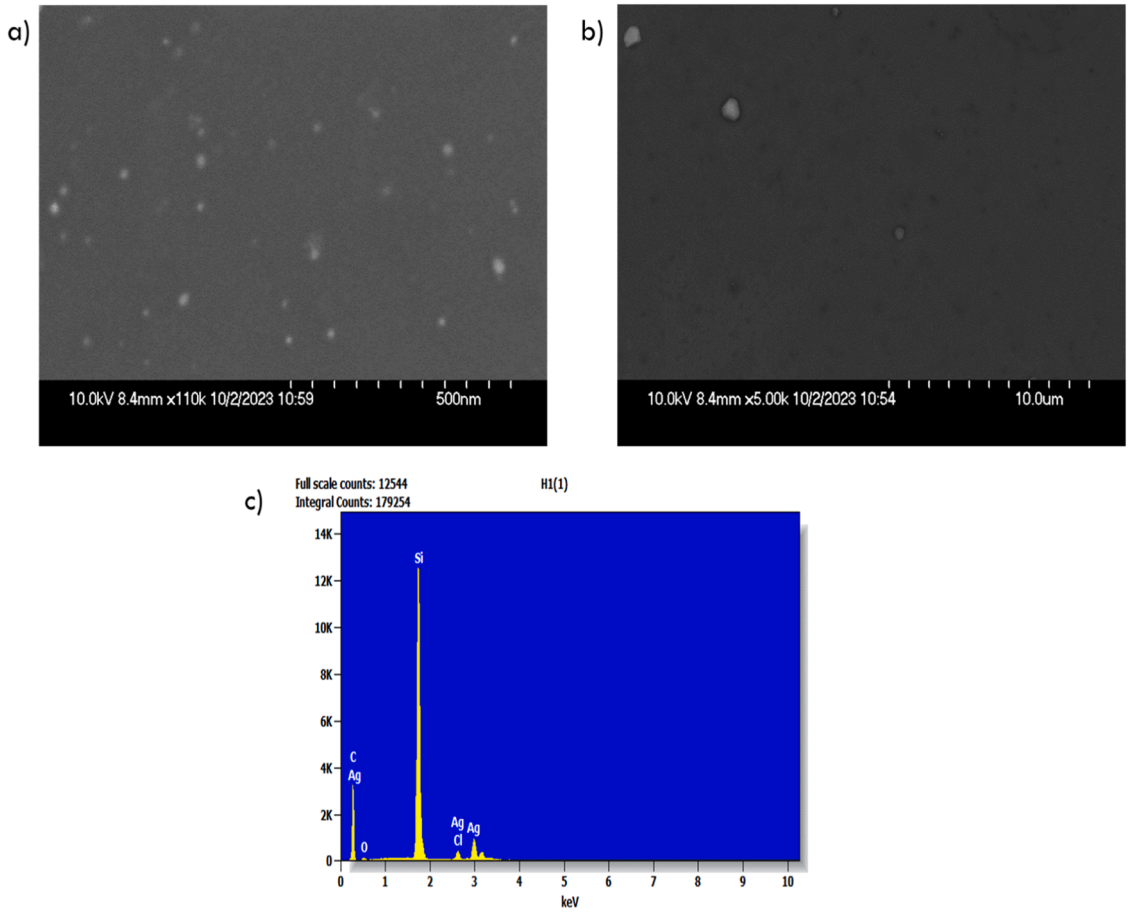

Fig. 4. FE-SEM micrograph of AgNPs at different magnification ranges (a) 10 μm, (b)500 nm, and (c) EDAX spectrum of Ag NPs.

Table 3
Result of EDAX spectrum with elemental composition.

Element	Weight %	Norm. Wt. %	Atom %	Compnd %
C	37.70	37.69	63.43	37.70
O	1.72	1.72	2.17	1.72
Si	41.77	41.77	30.06	41.77
Cl	2.14	2.14	1.22	2.14
Ag	16.68	16.68	3.13	16.68
Total	100.00	100.00	100.00	100.00

agglomeration indicates successful stabilization and dispersion of the nanoparticles. Surface plasmon resonance is responsible for the strong signal detected in the EDX data at roughly 0.2, 2.7, and 2.98 KeV, which indicates the presence of metallic silver nanocrystals. The other strong signals represent carbon, chloride, and oxygen absorption [44]. As shown in Fig. 4(c), this suggests that the phytochemical components of the *C. roseus* aqueous extract are present on the surface of AgNPs as a capping ligand.

XRD analysis

The XRD analysis of the AgNPs exhibited three prominent peaks at 2θ angles of 38.21°, 44.44°, and 64.7°, corresponding to spacing values of 2.354, 2.037, and 1.439, respectively, as shown in Fig. 5. These peaks are indicative of the face-centered cubic (FCC) structure of metallic silver, precisely corresponding to the crystallographic planes (111), (200), and (220). According to the Debye-Scherrer equation, the average size of AgNPs was found to be 22 nm, consistent with previous reports [45].

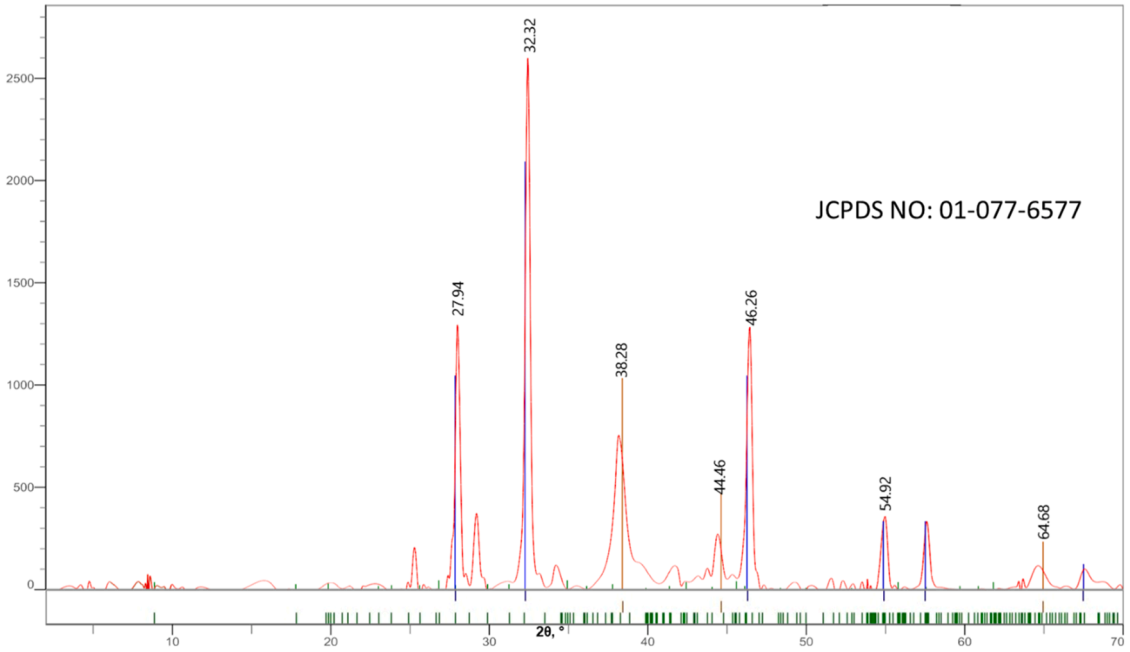

Fig. 5. XRD patterns of silver nanoparticles.

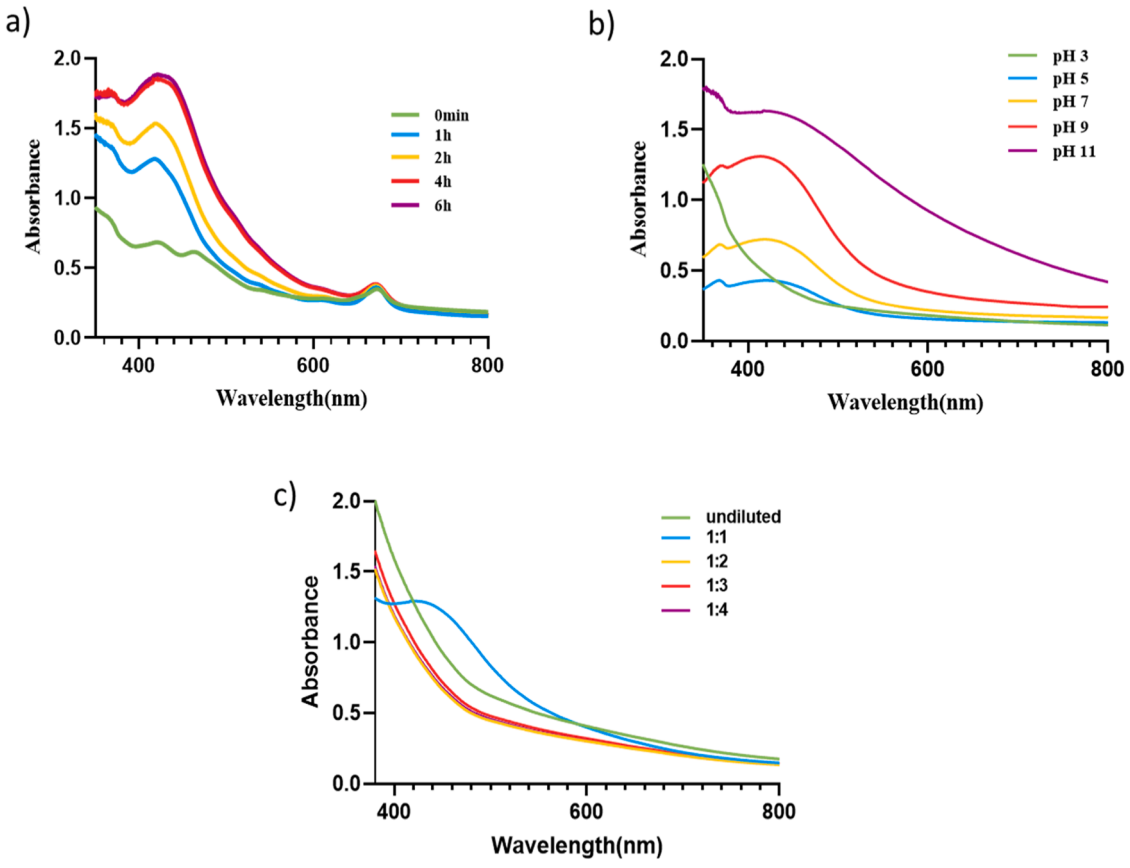

Fig. 6. UV-visible spectra of silver nanoparticle synthesis under various conditions: (a) different time incubations, (b) pH, and (c) aqueous extract dilutions.

Optimization of biosynthesis of silver nanoparticles

The UV–Vis spectroscopy data for silver nanoparticles (AgNPs) shows that a surface plasmon resonance (SPR) peak emerges rapidly within the first 30 min, indicating the initial formation of AgNPs. However, it is at the 6 h mark that a distinct SPR peak at 429 nm is observed, which is highly specific for AgNPs. The UV–Vis spectrum after 6 h indicated no further change in absorbance, confirming that the most efficient reaction time was 6 h and the quantity of silver nanoparticles increased with the time of exposure, and the shape of the particles might have been deviated from the ideal spherical geometry [46], as depicted in Fig. 6(a). The UV–Vis spectra of AgNPs produced in acidic conditions at pH 3 demonstrated that acidic conditions were unfavorable for AgNP production. Additionally, the AgNPs solution exhibited a lightened color in the acidic medium.

Conversely, a broad peak at pH 5 and 7 indicated the establishment of nonuniform particle sizes [29]. At pH 11, nanoparticle agglomeration was observed. Therefore, the pH 9, with 6 h of incubation, showed maximum absorbance at 416 nm, to form AgNPs with higher yield and smaller size, as shown in Fig. 6(b).

The impact of the quantity of *C. roseus* extract on the synthesis of AgNPs was investigated at a 1 mM $AgNO_3$. The UV–visible absorption peak analysis successfully demonstrated the synthesis of AgNPs in a 1:1 diluted extract, as shown in Fig. 6(c). No absorption peaks were observed in undiluted, 1:2, 1:3, and 1:4 ratios. In cases of an excessively high extract ratio, absorption peaks either overlapped with those of AgNPs or, in extreme scenarios, led to the absence of nanoparticle formation [47], lead to a reduction in the stability of the nanoparticles and the formation of larger-sized particles nanoparticles due to the agglomeration of particles in response to higher concentrations of reducing metabolites present in the plant extract [48].

Stability study

At pH 3, UV–visible spectra showed no absorption peak, indicating that the AgNPs are unstable. At pH 5 and 7, the peaks become broader, and the size of particles increases. The broad peak at pH 11 indicates the formation of nonuniform particle size. At a pH of 9, there is an increase in absorption, resulting in a narrow peak with a consistent distribution of size [49]. The pH 9 is the optimal pH for maintaining the stability of AgNPs, as shown in Fig. 7(a). These results align with Khan et al. [28] that pH 9 is the optimal pH for maintaining the stability of AgNPs. The synthesized AgNPs were assessed for heat stability ranging from 25 to 100 °C by exposing the

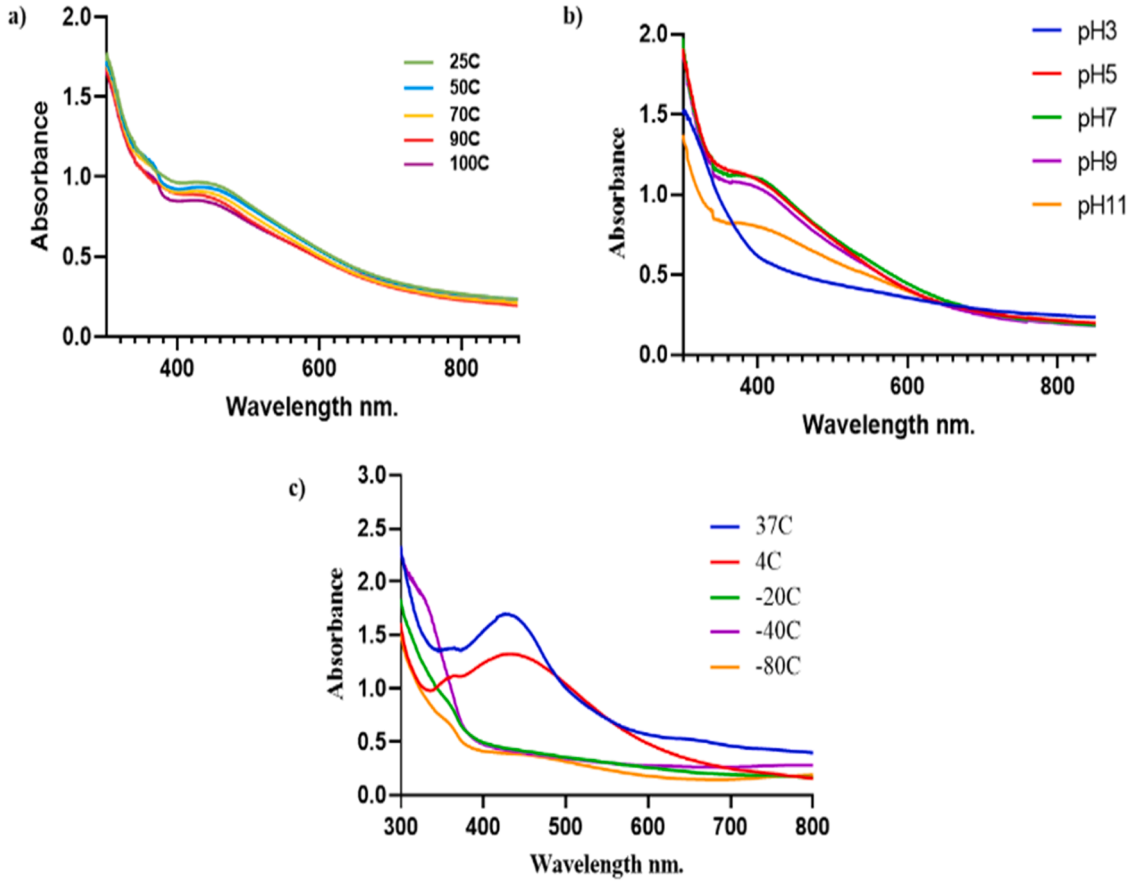

Fig. 7. The UV–visible spectrum illustrates the impact of (a) temperature, (b) pH variations, and (c) storage conditions on the stability of AgNPs.

AgNPs to various temperatures for 30 minutes, as illustrated in Fig. 7(b). At 25 °C, the peak with the highest intensity (429 nm) was observed. However, as the temperature increased, a noticeable decline in absorbance was observed. The peaks broadened at 100 °C, indicating that the AgNPs are unstable and began to degrade under high-temperature condition [50]. It suggests that AgNPs tend to become polydispersed with an increase in temperature beyond 25 °C [29]. The storage stability of synthesized AgNPs was investigated over 4 months at various temperatures (37, 4, −20, −40, and −80 °C), as depicted in Fig. 7(c). At 37 °C, the AgNPs displayed high stability, with the highest intensity peak observed at 450 nm. However, as the temperature decreased to 4 °C, a reduction in stability was observed, accompanied by a broadening of the peak. At −20, −40, and −80 °C, showcasing their robust stability at 37 °C , while at low-temperature conditions the AgNPs exhibited a lack of stability. This characteristic eliminates the need for refrigeration to maintain the stability of the AgNPs, showcasing their robust stability at physiological temperatures. In contrast, chemically synthesized AgNPs often suffer from stability issues due to aggregation, oxidation, and the use of toxic and flammable reducing and stabilizing agents, which can reduce nanoparticle stability [51,52].

Antiproliferative & cytotoxic activity

In this study, the blind assessment of the antiproliferative activity of AgNPs and an aqueous extract of *C. roseus* against HeLa229 cell lines at 200 µg/ml revealed intriguing findings (Supplementary Figure S2). Notably, the AgNPs exhibited less than 50 % cell viability, indicating a substantial inhibitory effect on HeLa229 cell proliferation at this concentration. In contrast, the aqueous extract demonstrated a significantly higher cell viability of 87 %, suggesting a comparatively lower cytotoxicity effect when compared to the AgNPs, suggesting a potentially enhanced cytotoxicity associated with the synthesized silver nanoparticles [53]. Therefore, to determine the IC_{50} for the AgNPs, a 2-fold serial dilution approach will be employed.

The inhibition of cell proliferation by the AgNPs and vincristine sulfate is illustrated in Fig. 8(a,b), with the IC_{50} of AgNPs calculated at 64.44 µg/ml at 24 h and 44.53 µg/ml at 48 h. Vincristine sulfate (standard reference drug) exhibited an IC_{50} of 92.02 µg/ml at 24 h and 91.07 µg/ml at 48 h. A significant difference ($^{***}P = 0.0001$, $^{**}P < 0.0063$) was observed when comparing the two treatments, as detailed in Table 4. Therefore, AgNPs exhibit effective cytotoxicity against HeLa cancer cells due to smaller-sized particles. Smaller sized silver nanoparticles have been shown to exhibit a higher level of cytotoxicity [53]. Meanwhile, Ghozali et al. [54] reported that the synthesized C. roseus-AgNPs exhibit more toxicity on Jurkat cells and HT-29 cells than the aqueous extract of C. roseus. In

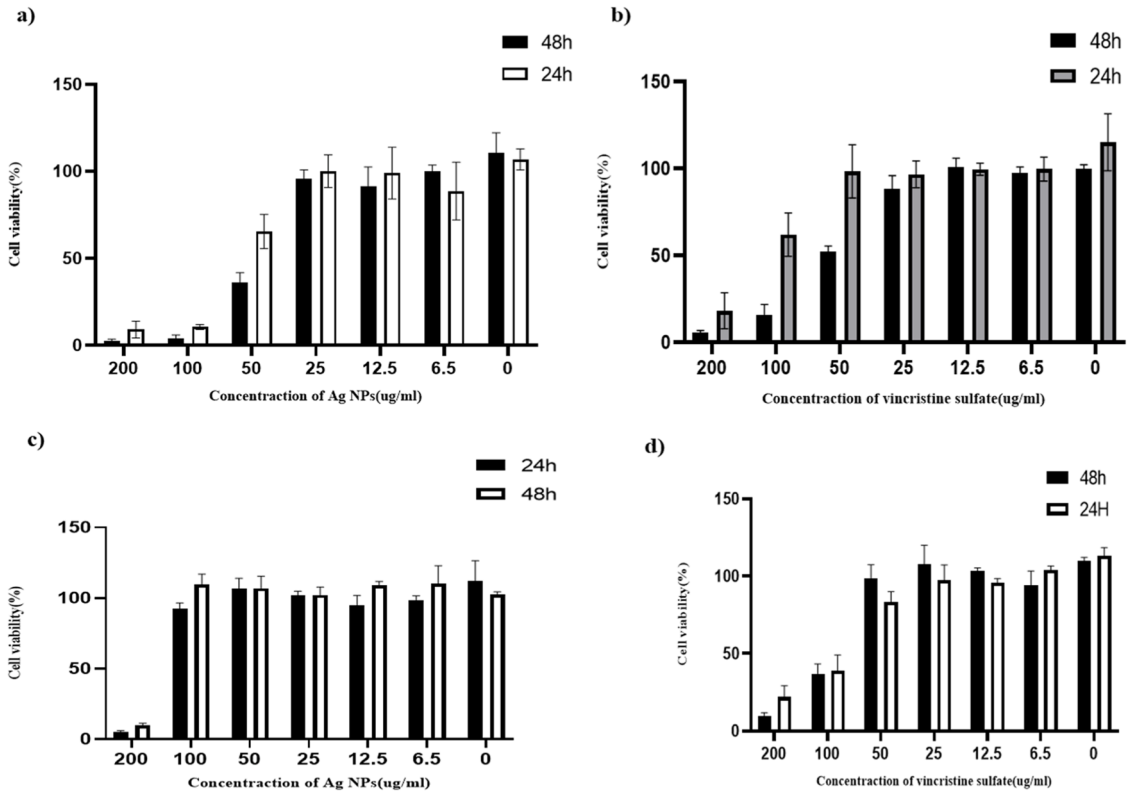

Fig. 8. (a) inhibition concentration (IC_{50}) of AgNPs, and (b) vincristine sulfate in HeLa229 cell lines. (c) Cytotoxic concentration effect (CC_{50}) of AgNPs, and (d) vincristine sulfate against Vero ccl-81 cells: both cell lines were treated with serial concentrations (200, 100, 50, 25, 12.25, and 6.25 µg/ml) of AgNPs and vincristine sulfate for 24 and 48 h, to determine the IC_{50} and CC50. Values are expressed as mean ± SEM. All treatments were conducted in triplicate. Significant differences between treatments are denoted: $^{***}P = 0.0001$, $^{**}P < 0.0063$ (IC_{50} comparison), and ***P<0.0005, $^{**}P < 0.0010$ (CC_{50} comparison).

Table 4
Summary of IC_{50}, CC_{50} and selectivity index values of AgNPs and vincristine sulfate.

	Treatment			
	AgNPs		Vincristine sulfate	
	24h	48h	24h	48h
IC_{50}(μg/ml)	64.44±3.64	44.53±2.08	92.02±1.20	91.07±1.16
CC_{50}(μg/ml)	202.5 ± 2.13	274.8 ± 2.17	119.9 ± 3.92	111.4 ± 1.58
SI	3.14	6.17	1.30	1.22

comparison, AgNPs synthesized through non-biological methods, such as chemical reduction with dextrose or encapsulation using polyethylene glycol, have demonstrated less effective anticancer activities against HeLa cell lines [55].

The in-vitro safety profile of AgNPs and vincristine sulfate was further assessed on Vero ccL-81 cells (Normal cells), as displayed in Fig. 8(c,d). The cytotoxic concentration (CC_{50}) for AgNPs was 202.5 μg/ml at 24 h and 274.8 μg/ml at 48 h, demonstrating significant differences (***P < 0.0005, **P < 0.0010) compared to vincristine sulfate, as indicated in Table (4). Meanwhile, Khansa et al. [25] found AgNPs to have positive potential on the Vero cell line.

Selectivity index (SI)

Table (4) presents the calculated selectivity index (SI) for AgNPs, with values of 3.14 and 6.17 at 24 and 48 h, respectively. In comparison, Vincristine sulfate exhibited SI values of 1.30 and 1.22 at 24 and 48 h, respectively. The study found that AgNPs showed higher selective antiproliferative effect on cervical (HeLa 229) cell line without affecting non-cancerous ones (Vero ccL-81) than vincristine sulfate (Reference drug).

The higher selectivity of AgNPs suggests a more targeted and specific antiproliferative effect on HeLa cancer cell, while biocompatible and low-toxicity on Vero cell. This enhanced selectivity is attributed to the natural compounds present in Catharanthus roseus, which reduce potential risks associated with cytotoxic effects on normal cells. In contrast, chemically synthesized AgNPs may pose cytotoxic effects due to the use of toxic reducing agents [26].

Wound healing assay

Metastasis is a critical and formidable challenge in cancer treatment [49]. Cervical cancer, characterized by significant metastatic potential, has witnessed a surge in mortality rates. HeLa 229 cell lines were treated with the IC_{50} concentrations AgNPs. After edge progression for 24, 48, and 72 h, residual scar areas were compared to the initial gap area to calculate the wound closure percentage. The results in Fig. 9(a) reveal that AgNPs can impede cell wound progression by approximately 16.67 %, 29.24 %, and 33.22 % at 24, 48, and 72 h, respectively. (****P < 0.0001) indicates a high level of significance. In comparison, vincristine sulfate (Reference drug) demonstrated inhibition percentages of 21.62 %, 47.73 %, and 54.09 % at 24, 48, and 72 h, respectively, demonstrating significant differences (****P < 0.0001) compared to a control group, as shown in Fig. 9(b). It suggests that AgNPs of *C. roseus* possess significant potential as antimetastatic agents by inhibiting cancer cell migration. As a promising therapeutic agent for impeding cancer cell migration, AgNPs demonstrate higher antimetastatic efficacy than vincristine sulfate, suggesting that AgNPs have a notable impact on limiting the movement and migration of cells, which is a critical factor in the metastatic process.

Gene expression analysis

The mRNA expression levels for significant genes (p21, CDK1, p53, BCL-2, and Caspase-9) were evaluated using RT-qPCR to explore their role in cancer treatment and carcinogenesis, namely in cell survival and dysregulation of apoptosis [56]. To standardize the relative mRNA expression levels of the target genes, β-Actin was employed as a reference, as depicted in Fig. 10.

After subjecting cells to AgNPs treatment for 24 and 48 h, a significant downregulation in the mRNA expression of BCL-2 and CDK1 was observed. Notably, BCL-2 displayed a noteworthy reduction after 48 hours (**P = 0.0043), although no statistical significance was found in BCL-2 downregulation after 24 h (P = 0.0898). On the other hand, CDK1 showed a highly significant downregulation at both time points (****P < 0.0001, ****P < 0.0001). Furthermore, there was a significant upregulation in the expression levels of p53, p21, and caspase9 (****P < 0.0001, ****P < 0.0001) at both time points, suggesting a coordinated response to AgNPs treatment. In contrast, treatment with vincristine sulfate (reference drug) resulted in a substantial downregulation of BCL-2 (***P = 0.0006, **P = 0.00018) and CDK1 (*P = 0.0396, **P < 0.0028) at both 24 and 48 hours. Additionally, there was a significant upregulation in the expression levels of caspase9 (*P = 0.0396, ****P < 0.0001). After 24 and 48 hours, there was no statistically significant difference in the increase of p21 expression (P = 0.999, P = 0.529), and p53 upregulation after 24 hours (P = 0.3196) but after 48 hours showed a significant difference (**P = 0.0014). These findings underscore the differential molecular responses induced by AgNPs of *C. roseus* and vincristine sulfate, offering valuable insights into their potential mechanisms of action over distinct time intervals.

The changes in gene expression levels in the HeLa229 cancer cell line after treatment with AgNPs suggest a potential anti-cancer effect mediated through alterations in apoptosis and cell cycle regulation. The downregulation of BCL-2, particularly after 48 hours of treatment, is noteworthy in the context of cancer cells. BCL-2′s anti-apoptotic function is often exploited by cancer cells to resist

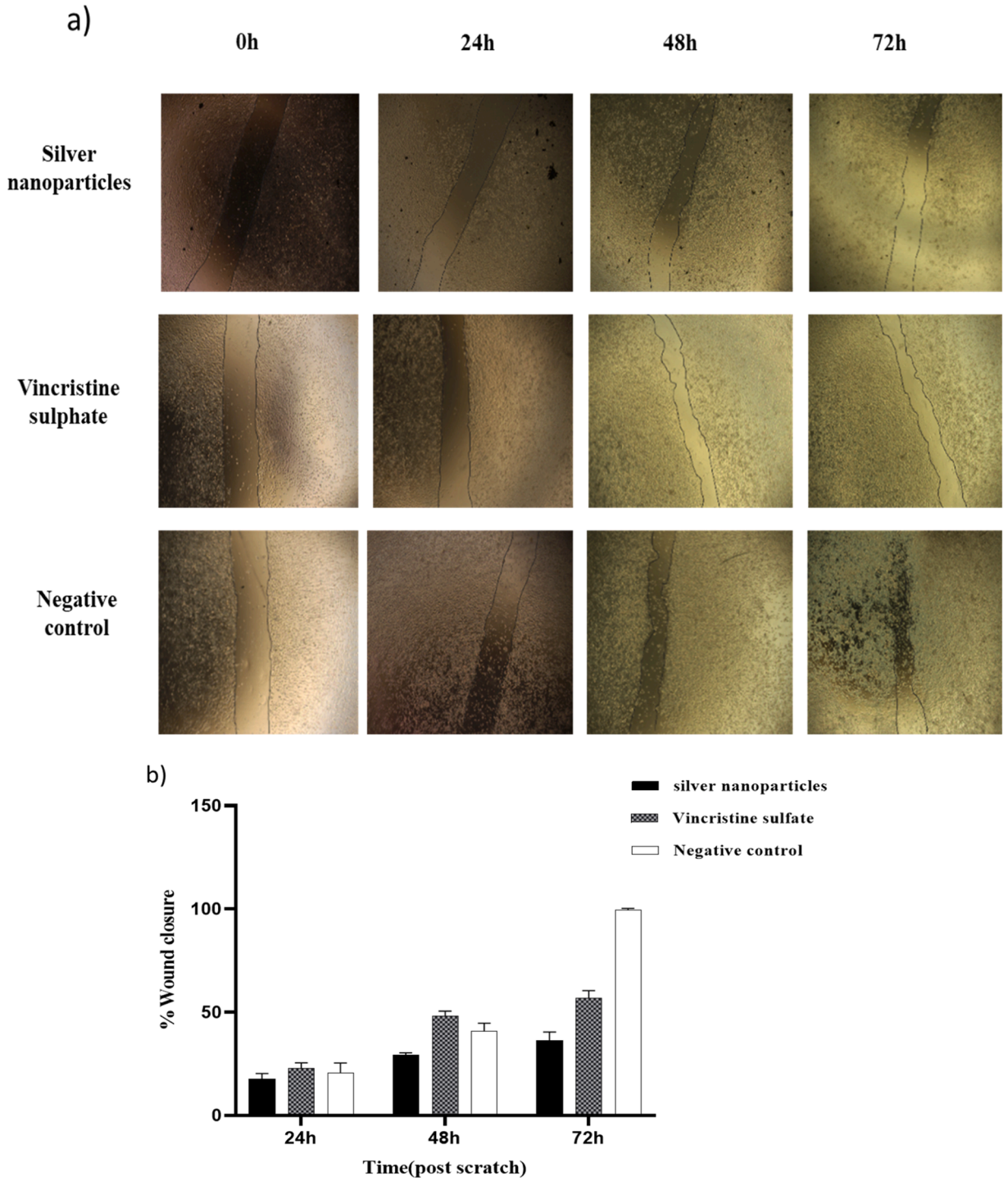

Fig. 9. (a) Representative images from wound healing assay of HeLa229 cell line (b) percentage wound closure at different time points: wound healing assays were conducted on HeLa 229 cell lines treated with AgNPs for 24, 48, and 72 h. Representative images were captured using an EVOS microscope. The wound areas were quantified using Image J software, significant differences(****$P < 0.0001$) compared to a negative control.

programmed cell death [57]. The significant decrease in BCL-2 expression indicates a potential disruption of this anti-apoptotic defense mechanism, making HeLa229 cells more susceptible to apoptosis [58]. The differences observed in BCL-2 downregulation after 48 h compared to 24 h may suggest that the impact of AgNPs on BCL-2 expression takes time to manifest. The upregulation of p53 is a crucial observation, as p53 acts as a tumor suppressor by orchestrating responses to cellular stress, including DNA damage. The

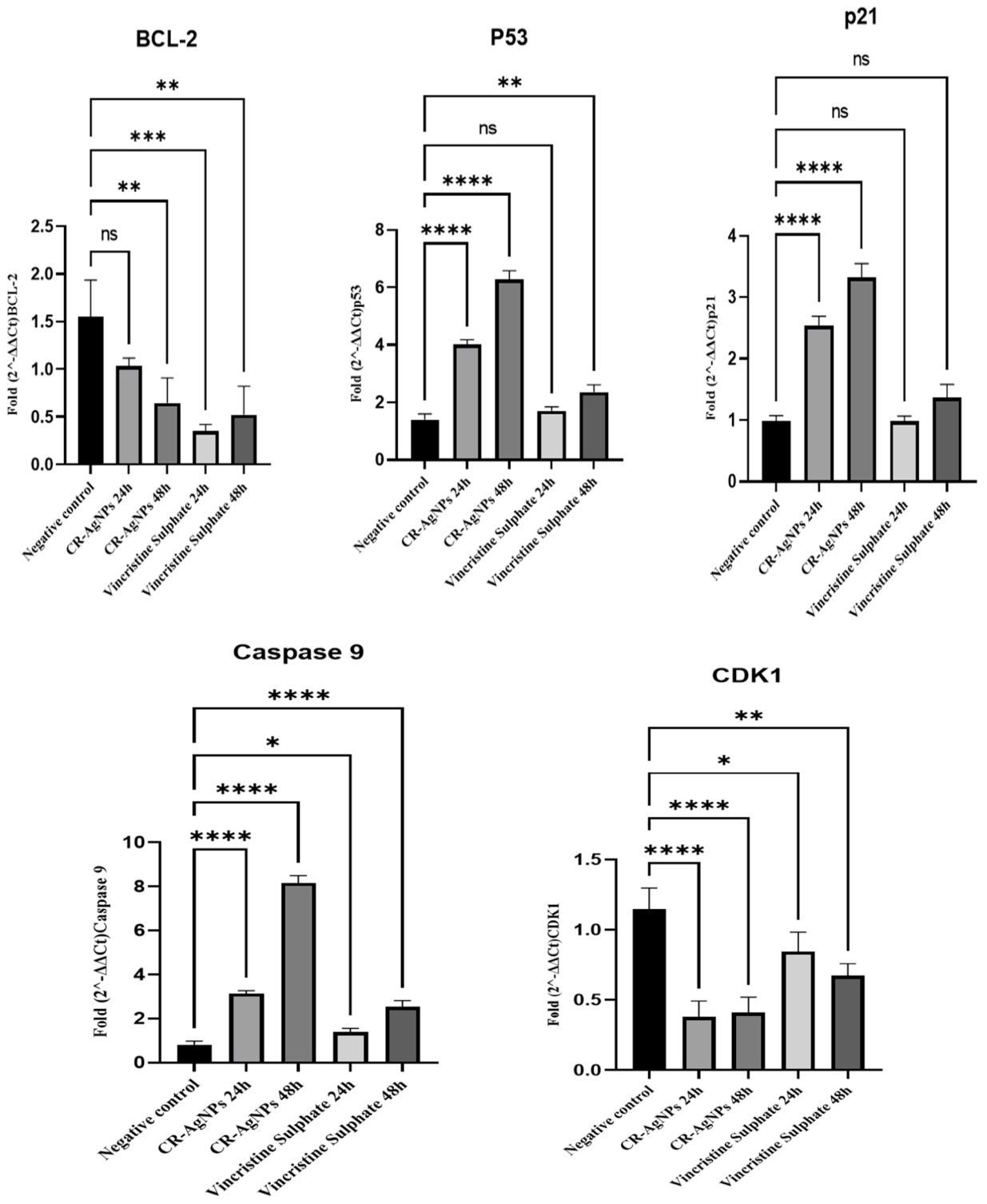

Fig. 10. bar graph illustrating the relative gene expression analysis of cell cycle-related genes (p21 and CDK1) and apoptosis-related genes (p53, Bcl-2, and Caspase9) following a 24 and 48-hour treatment of the HeLa229 cell line with AgNPs and vincristine sulfate. Values are expressed as Mean ± SEM.

increased p53 expression over 24 and 48 h suggests that AgNPs induce and maintain a cellular stress response in HeLa229 cells. This activation can lead to the initiation of apoptosis or cell cycle arrest, contributing to anti-cancer effects. The concurrent upregulation of p21, a downstream target of p53, supports the notion of cell cycle arrest [59]. By inhibiting CDKs, p21 can halt the cell cycle progression, preventing uncontrolled cell division. It is particularly relevant in cancer cells, where unregulated cell cycle progression is a hallmark feature. The downregulation of CDK1 is consistent with the observed cell cycle-related effects [60]. CDK1 is a crucial cell cycle regulator, and its decreased expression suggests a potential inhibition of cell proliferation [61]. This outcome corresponds to the antiproliferative and anti-survival effects in HeLa229 cancer cells treated with AgNPs. The upregulation of caspase9 further reinforces the potential induction of apoptosis [62]. Caspase9 is a critical initiator caspase in the intrinsic apoptotic pathway, and its increased expression implies the activation of apoptotic cascades in HeLa229 cells treated with AgNPs. The combined effects on BCL-2, p53, p21, CDK1, and caspase9 suggest a multi-faceted impact on HeLa229 cells. The downregulation of anti-apoptotic and pro-survival factors (BCL-2, CDK1) and the upregulation of pro-apoptotic and cell cycle checkpoint factors (p53, p21, caspase9) collectively indicate a shift towards apoptosis and cell cycle arrest in response to silver nanoparticles. These results suggest that AgNPs of *C. roseus* have potential as anti-cancer agents by inducing oxidative stress, resulting in mitochondrial damage and subsequent activation of the intrinsic apoptosis pathway. Additionally, AgNPs can induce cell cycle arrest through the mediation of p53 activation and upregulation of p21 [63,64].

The vincristine sulfate (Reference drug) showed downregulation of BCL-2 and CDK1, similar to AgNPs, indicating an anti-survival effect and inhibition of cell proliferation. The observed upregulation of caspase9 suggests an induction of apoptosis, which aligns with the downregulation of BCL-2 [65]. Unlike AgNPs, vincristine sulfate did not show a significant upregulation of p21 after 24 and 48 h. Furthermore, the increase in p53 expression after 48 h indicates a response that depends on time, possibly associated with the drug's mechanism of action.

Conclusion

In conclusion, this study successfully demonstrated the efficient biosynthesis of silver nanoparticles of *C. roseus* aqueous extract. The AgNPs exhibited a well-defined spherical morphology with an average size ranging from 6 to 33 nm. The AgNPs displayed remarkable antiproliferative and antimetastatic activities against cervical (HeLa229) cell lines by inducing apoptosis and arresting the cell cycle. The study confirms that the synthesis of silver nanoparticles using *C. roseus* enhances the anticancer activity of the *C. roseus* extract, leading to improved therapeutic outcomes. The promising characteristics of AgNPs, such as their good selectivity index, size, and stability, position them as a novel and safe alternative for cervical cancer treatment. Nevertheless, the transition from in vitro findings to clinical applications necessitates further in vivo research to enhance our understanding of AgNP's efficacy, safety, and potential mechanisms of action. These efforts will be pivotal in advancing the translational potential of AgNPs for cervical cancer therapy.

CRediT authorship contribution statement

Hadil S. Hussein: Methodology, Formal analysis, Investigation, Resources, Writing – original draft, Visualization. **Caroline Ngugi:** Writing – review & editing, Supervision. **Festus M. Tolo:** Writing – review & editing, Supervision. **Esther N. Maina:** Writing – review & editing, Supervision.

Declaration of competing interest

The authors declare no conflict of interest exists with this manuscript.

Acknowledgments

We want to express our sincere gratitude to the Pan African University Institute for Basic Sciences, Technology, and Innovation (PAUSTI), the Centre for Traditional Medicine and Drug Research, Kenya Medical Research Institute (KEMRI), and Jomo Kenyatta University of Agriculture and Technology for their contributions.

Funding

The African Union scholarship program funded this research through the Pan African University Institute for Basic Sciences, Technology, and Innovation (PAUSTI).

Supplementary materials

Supplementary material associated with this article can be found, in the online version, at doi:10.1016/j.sciaf.2024.e02268.

References

[1] S.V.S. Deo, J. Sharma, S. Kumar, GLOBOCAN 2020 report on global cancer burden: challenges and opportunities for surgical oncologists, Ann. Surg. Oncol. 29 (11) (2022) 6497–6500, https://doi.org/10.1245/s10434-022-12151-6.

[2] H. Sung, et al., Global cancer statistics 2020: GLOBOCAN estimates of incidence and mortality worldwide for 36 cancers in 185 countries, CA. Cancer J. Clin. 71 (3) (2021) 209–249, https://doi.org/10.3322/caac.21660.

[3] R. Sharma, et al., Mapping cancer in Africa: a comprehensive and comparable characterization of 34 cancer types using estimates from GLOBOCAN 2020, Front. Public Heal. 10 (2022) 839835, https://doi.org/10.3389/fpubh.2022.839835.

[4] X. Wang, et al., Ag nanoparticles immobilized on guanidine modified-KIT-5 mesoporous nanostructure: evaluation of its catalytic activity for synthesis of propargylamines and investigation of its antioxidant and anti-lung cancer effects, Arab. J. Chem. 15 (2) (2022) 103548, https://doi.org/10.1016/j.arabjc.2021.103548.

[5] Z. Chang, et al., Preparation of gelatin/Ag NPs under ultrasound condition: a potent and green bio-nanocomposite for the treatment of pleomorphic hepatocellular carcinoma, morris hepatoma, and novikoff hepatoma, Arab. J. Chem. 15 (6) (2022) 103858, https://doi.org/10.1016/j.arabjc.2022.103858.

[6] Y. Cai, et al., Oak gum mediated green synthesis of silver nanoparticles under ultrasonic conditions: characterization and evaluation of its antioxidant and anti-lung cancer effects, Arab. J. Chem. 15 (6) (2022) 103848, https://doi.org/10.1016/j.arabjc.2022.103848.

[7] Y. Cai, et al., Ag NPs supported chitosan-agarose modified Fe3O4 nanocomposite catalyzed synthesis of indazolo[2,1-b]phthalazines and anticancer studies against liver and lung cancer cells, Int. J. Biol. Macromol. 208 (February) (2022) 20–28, https://doi.org/10.1016/j.ijbiomac.2022.02.172.

[8] A.I. Felimban, N.S. Alharbi, N.S. Alsubhi, Optimization, characterization, and anticancer potential of silver nanoparticles biosynthesized using Olea europaea, Int. J. Biomater. 2022 (2022), https://doi.org/10.1155/2022/6859637.

[9] G.S. Vuanghao L, Biosynthesis and characterization of silver nanoparticles using catharanthus roseus leaf extract and its proliferative effects on cancer cell lines, J. Nanomed. Nanotechnol. 06 (04) (2015), https://doi.org/10.4172/2157-7439.1000305.

[10] K.S. Allemailem, et al., applied sciences Ajwa-dates (Phoenix dactylifera) -mediated synthesis of silver cytotoxic potential, Appl. Sci. (2022).

[11] H. Rouhollah, Biological applications of biosynthesized silver nanoparticles through the utilization of plant extracts, Herb. Med. J. 2 (2) (2017) 87–95, https://doi.org/10.22087/hmj.v0i0.618.

[12] A. Binod, S.V. Ganachari, J.S. Yaradoddi, R.P. Tapaskar, N.R. Banapurmath, A.S. Shettar, Biological synthesis and characterization of tri- metallic alloy (Au Ag, Sr) nanoparticles and its sensing studies, in: IOP Conference Series: Materials Science and Engineering 376, 2018, https://doi.org/10.1088/1757-899X/376/1/012054.

[13] L.B. Anigol, V.P. Sajjan, P.M. Gurubasavaraj, S.V. Ganachari, D. Patil, Study on the effect of pH on the biosynthesis of silver nanoparticles using Capparis moonii fruit extract: their applications in anticancer activity, biocompatibility and photocatalytic degradation, Chem. Pap. 77 (6) (2023) 3327–3345, https://doi.org/10.1007/s11696-023-02707-5.

[14] S.H. Salmen, S.A. Alharbi, Silver nanoparticles synthesized biogenically from Aloe fleurentiniorum extract: characterization and antibacterial activity, Green Chem. Lett. Rev. 13 (1) (2020) 1–5, https://doi.org/10.1080/17518253.2019.1707883.

[15] L. Wang, B. Karmakar, F.A. Al-Saeed, A.A. Shati, M.Z. Bani-Fwaz, A.F. El-kott, Green synthesis of Ag/Fe3O4 nanoparticles using Mentha longifolia flower extract: evaluation of its antioxidant and anti-lung cancer effects, Heliyon 8 (12) (2022), https://doi.org/10.1016/j.heliyon.2022.e12326.

[16] S.M. Anjum, K. Riazunnisa, Fine ultra-small ruthenium oxide nanoparticle synthesis by using catharanthus roseus and moringa oleifera leaf extracts and their efficacy towards in vitro assays, antimicrobial activity and catalytic: adsorption kinetic studies using methylene blue dye, J. Clust. Sci. 33 (3) (2022) 1103–1117, https://doi.org/10.1007/s10876-021-02037-0.

[17] H.N.T. Pham, Q. Van Vuong, M.C. Bowyer, C.J. Scarlett, Phytochemicals derived from catharanthus roseus and their health benefits, Technologies 8 (4) (2020) 80, https://doi.org/10.3390/technologies8040080.

[18] B.V. Bonifácio, P.B. da Silva, M. Aparecido dos Santos Ramos, K. Maria Silveira Negri, T. Maria Bauab, M. Chorilli, Nanotechnology-based drug delivery systems and herbal medicines: a review, Int. J. Nanomedicine 9 (1) (2013) 1–15, https://doi.org/10.2147/IJN.S52634.

[19] S.S. Ajazuddin, Applications of novel drug delivery system for herbal formulations, Fitoterapia 81 (7) (2010) 680–689, https://doi.org/10.1016/j.fitote.2010.05.001.

[20] S.H. Ansari, F. Islam, M. Sameem, Influence of nanotechnology on herbal drugs: a review, J. Adv. Pharmaceut. Technol. Res. 3 (3) (2012) 142–146, https://doi.org/10.4103/2231-4040.101006.

[21] T.V.M. Sreekanth, M. Pandurangan, D.H. Kim, Y.R. Lee, Green synthesis: in-vitro anticancer activity of silver nanoparticles on human cervical cancer cells, J. Clust. Sci. 27 (2) (2016) 671–681, https://doi.org/10.1007/s10876-015-0964-9.

[22] K. Kabesh, P. Senthilkumar, R. Ragunathan, R.R. Kumar, Phytochemical analysis of *Catharanthus roseus* plant extract and its antimicrobial activity, Int. J. Pure Appl. Biosci. 3 (2) (2015) 162–172.

[23] L.V. Hublikar, S.V. Ganachari, V.B. Patil, S. Nandi, A. Honnad, Anticancer potential of biologically synthesized silver nanoparticles using Lantana camara leaf extract, Prog. Biomater. 12 (2) (2023) 155–169, https://doi.org/10.1007/s40204-023-00219-9.

[24] D. Chaudhary, A. Deep, N. Bansal, N. Rani, Methods of synthesis, characterization and anticancer potential of herbal silver nanoparticles: a review, Curr. Cancer Ther. Rev. 19 (4) (2023) 318–333, https://doi.org/10.2174/1573394719666230419095939.

[25] K. Jamil, et al., Biogenic synthesis of silver nanoparticles using catharanthus roseus and its cytotoxicity effect on vero cell lines, Molecules 27 (19) (2022) 1–18, https://doi.org/10.3390/molecules27196191.

[26] N. Jain, P. Jain, D. Rajput, U.K. Patil, Green synthesized plant-based silver nanoparticles: therapeutic prospective for anticancer and antiviral activity, Micro Nano Syst. Lett. 9 (1) (2021), https://doi.org/10.1186/s40486-021-00131-6.

[27] B. Mousavi, F. Tafvizi, S. Zaker Bostanabad, Green synthesis of silver nanoparticles using Artemisia turcomanica leaf extract and the study of anti-cancer effect and apoptosis induction on gastric cancer cell line (AGS), Artif. Cells, Nanomedicine Biotechnol. 46 (sup1) (2018) 499–510, https://doi.org/10.1080/21691401.2018.1430697.

[28] S. Khan, S. Singh, S. Gaikwad, N. Nawani, M. Junnarkar, S.V. Pawar, Optimization of process parameters for the synthesis of silver nanoparticles from Piper betle leaf aqueous extract, and evaluation of their antiphytofungal activity, Environ. Sci. Pollut. Res. 27 (22) (2020) 27221–27233, https://doi.org/10.1007/s11356-019-05239-2.

[29] N. Ahmad, et al., Green fabrication of silver nanoparticles using Euphorbia serpens Kunth aqueous extract, their characterization, and investigation of its in vitro antioxidative, antimicrobial, insecticidal, and cytotoxic activities, Biomed Res. Int. 2022 (2022), https://doi.org/10.1155/2022/5562849.

[30] M.R. Wardihan, G. Alam, Lukman, M.A. Manggau, Selective cytotoxicity evaluation in anticancer drug screening of Boehmeria virgata (Forst) guill leaves to, Dhaka Univ. J. Pharm. Sci. 12 (2) (2013) 87–90.

[31] J.T. Freitas, I. Jozic, B. Bedogni, Wound healing assay for melanoma cell migration, Methods Mol. Biol. 2265 (2021) 65–71, https://doi.org/10.1007/978-1-0716-1205-7_4.

[32] S. Goswami, Preliminary phytochemical screening and standardisation of leaves of Catharanthus Roseus (L .) G . Don, Indian J. Res. Pharm. Biotechnol. 1 (1) (2009) 24–27.

[33] R. Yadav, R.K. Khare, A. Singhal, Qualitative phytochemical screening of some selected medicinal plants of shivpuri district (M.P.), Int. J. Life-Sci. Sci. Res. 3 (1) (2017) 844–847, https://doi.org/10.21276/ijlssr.2017.3.1.16.

[34] S. Pirtarighat, M. Ghannadnia, S. Baghshahi, Green synthesis of silver nanoparticles using the plant extract of Salvia spinosa grown in vitro and their antibacterial activity assessment, J. Nanostruct. Chem. 9 (1) (2019) 1–9, https://doi.org/10.1007/s40097-018-0291-4.

[35] M.R. Bindhu, M. Umadevi, G.A. Esmail, N.A. Al-Dhabi, M.V. Arasu, Green synthesis and characterization of silver nanoparticles from Moringa oleifera flower and assessment of antimicrobial and sensing properties, J. Photochem. Photobiol. B Biol. 205 (2020) 32172135, https://doi.org/10.1016/j.jphotobiol.2020.111836.

[36] R.H. Ahmed, D.E. Mustafa, Green synthesis of silver nanoparticles mediated by traditionally used medicinal plants in Sudan, Int. Nano Lett. 10 (1) (2020) 1–14, https://doi.org/10.1007/s40089-019-00291-9.
[37] K.S. Mukunthan, E.K. Elumalai, T.N. Patel, V.R. Murty, Catharanthus roseus: a natural source for the synthesis of silver nanoparticles, Asian Pac. J. Trop. Biomed. 1 (4) (2011) 270–274, https://doi.org/10.1016/S2221-1691(11)60041-5.
[38] S. Ponarulselvam, C. Panneerselvam, K. Murugan, N. Aarthi, K. Kalimuthu, S. Thangamani, Synthesis of silver nanoparticles using leaves of Catharanthus roseus Linn. G. Don and their antiplasmodial activities, Asian Pac. J. Trop. Biomed. 2 (7) (2012) 574–580, https://doi.org/10.1016/S2221-1691(12)60100-2.
[39] T. Rajagopal, I.A.A. Jemimah, P. Ponmanickam, M. Ayyanar, Synthesis of silver nanoparticles using Catharanthus roseus root extract and its larvicidal effects, J. Environ. Biol. 36 (6) (2015) 1283–1289.
[40] M. Rafique, I. Sadaf, M.S. Rafique, M.B. Tahir, A review on green synthesis of silver nanoparticles and their applications, Artif. Cells, Nanomed. Biotechnol. 45 (7) (2017) 1272–1291, https://doi.org/10.1080/21691401.2016.1241792.
[41] H. Singh, J. Du, T.H. Yi, Kinneretia THG-SQI4 mediated biosynthesis of silver nanoparticles and its antimicrobial efficacy, Artif. Cells, Nanomed. Biotechnol. 45 (3) (2017) 602–608, https://doi.org/10.3109/21691401.2016.1163718.
[42] A.O. Pryskoka, A.V. Rudenko, L.S. Reznichenko, T.G. Gruzina, Z.R. Ulberg, I.S. Chekman, The antimicrobial activity of silver nanoparticles in vitro, Vìsnik Farm. 0 (2(82)) (2015) 54–58, https://doi.org/10.24959/nphj.15.2002.
[43] P. Moteriya, S. Chanda, Synthesis and characterization of silver nanoparticles using Caesalpinia pulcherrima flower extract and assessment of their in vitro antimicrobial, antioxidant, cytotoxic, and genotoxic activities, Artif. Cells, Nanomed. Biotechnol. 45 (8) (2017) 1556–1567, https://doi.org/10.1080/21691401.2016.1261871.
[44] E.S. Al-Sheddi, et al., Anticancer potential of green synthesized silver nanoparticles using extract of nepeta deflersiana against human cervical cancer cells (HeLA, Bioinorg. Chem. Appl. 2018 (2018), https://doi.org/10.1155/2018/9390784.
[45] S. Rajawat, M.M. Malik, Anticancer activity of green silver nanoparticles against He-La cervical cancer cell lines, Mater. Today Proc. 18 (2019) 841–847, https://doi.org/10.1016/j.matpr.2019.06.510.
[46] S.V. Ganachari, R. Bhat, R. Deshpande, A. Venkataraman, Extracellular biosynthesis of silver nanoparticles using fungi penicillium diversum and their antimicrobial activity studies, Bionanoscience 2 (4) (2012) 316–321, https://doi.org/10.1007/s12668-012-0046-5.
[47] T.E. Agustina, W. Handayani, C. Imawan, The UV-VIS spectrum analysis from silver nanoparticles synthesized using Diospyros maritima Blume. Leaves extract, Proc. 3rd KOBI Congr. Int. Natl. Conf. (KOBICINC2020) 14 (Kobicinc 2020) (2021) 411–419, https://doi.org/10.2991/absr.k.210621.070.
[48] L.V. Hublikar, et al., Biogenesis of silver nanoparticles and its multifunctional anti-corrosion and anticancer studies, Coatings 11 (10) (2021), https://doi.org/10.3390/coatings11101215.
[49] X. Guan, Cancer metastases: challenges and opportunities, Acta Pharm. Sin. B 5 (5) (2015) 402–418, https://doi.org/10.1016/j.apsb.2015.07.005.
[50] R. Bhat, S. Ganachari, R. Deshpande, G. Ravindra, A. Venkataraman, Rapid biosynthesis of silver nanoparticles using areca nut (Areca catechu) extract under microwave-assistance, J. Clust. Sci. 24 (1) (2013) 107–114, https://doi.org/10.1007/s10876-012-0519-2.
[51] A. Dhaka, S. Sharma, R. Trivedi, A review on biological synthesis of silver nanoparticles and their potential applications, Res. Chem. 6 (September) (2023) 101108, https://doi.org/10.1016/j.rechem.2023.101108.
[52] S.V. Ganachari, et al., Green nanotechnology for biomedical, food, and agricultural applications, Handb. Ecomater. 4 (2019) 2681–2698, https://doi.org/10.1007/978-3-319-68255-6_184.
[53] L.V. Hublikar, S.V. Ganachari, V.B. Patil, Phytofabrication of silver nanoparticles using Averrhoa bilimbi leaf extract for anticancer activity, Nanoscale Adv. 5 (16) (2023) 4149–4157, https://doi.org/10.1039/d3na00313b.
[54] V. L, A.N. Ghozali SZ, Biosynthesis and characterization of silver nanoparticles using catharanthus roseus leaf extract and its proliferative effects on cancer cell lines, J. Nanomed. Nanotechnol. 06 (04) (2015), https://doi.org/10.4172/2157-7439.1000305.
[55] E.S.M.M. Rocio Casañas Pimentel, G.-G. & Q.G.A. Palacios, and C. Alberto Monroy García, “Silver nanoparticles nanocarriers , synthesis and toxic effect on cervical cancer cell lines,” pp. 1–9, 2013.
[56] I.O. Okpako, F.A. Ng’ong’a, C.M. Kyama, S.N. Njeru, Antiproliferative activity of ethyl acetate fraction of Euphorbia ingens against prostate cancer cell line: an in silico and in vitro analysis, Sci. Afr. 22 (May) (2023) 1–20, https://doi.org/10.1016/j.sciaf.2023.e01943.
[57] K.J. Campbell, S.W.G. Tait, Targeting BCL-2 regulated apoptosis in cancer, Open Biol. 8 (5) (2018) 1–11, https://doi.org/10.1098/rsob.180002.
[58] X. Chang, et al., Silver nanoparticles induced cytotoxicity in HT22 cells through autophagy and apoptosis via PI3K/AKT/mTOR signaling pathway, Ecotoxicol. Environ. Saf. 208 (2021) 22–23, https://doi.org/10.1016/j.ecoenv.2020.111696.
[59] R.M. Abdel-Megeed, S.A. Ali, W.B. Khalil, E.A. Refaat, M.O. Kadry, Mitigation of apoptosis-mediated neurotoxicity induced by silver nanoparticles via rutaceae nutraceuticals: P53 activation and Bax/Bcl-2 regulation, Toxicol. Rep. 9 (2022) 2055–2063, https://doi.org/10.1016/j.toxrep.2022.11.009.
[60] S.A. Abdelrahman, A.A. Mahmoud, A.A. Abdelrahman, W. Samy, E. Zaid Hassen Saleh, Histomorphological changes and molecular mechanisms underlying the ameliorative effect of resveratrol on the liver of silver nanoparticles-exposed rats, Ultrastruct. Pathol. 46 (3) (2022) 268–284, https://doi.org/10.1080/01913123.2022.2067929.
[61] N.R. Brown, et al., CDK1 structures reveal conserved and unique features of the essential cell cycle CDK, Nat. Commun. 6 (2015) 1–12, https://doi.org/10.1038/ncomms7769.
[62] J. Baharara, F. Namvar, T. Ramezani, M. Mousavi, R. Mohamad, Silver nanoparticles biosynthesized using Achillea biebersteinii flower extract: apoptosis induction in MCF-7 cells via caspase activation and regulation of bax and bcl-2 gene expression, Molecules 20 (2) (2015) 2693–2706, https://doi.org/10.3390/molecules20022693.
[63] Y. Yuan, S. Zhang, J. Hwang, I. Kong, Silver nanoparticles potentiates cytotoxicity and apoptotic potential of camptothecin in human cervical cancer cells, Hindawi 2018 (2018).
[64] G. Kah, R. Chandran, Biogenic silver nanoparticles for targeted cancer therapy and enhancing photodynamic therapy, Cells (2023).
[65] J.L. Hsu, W.J. Leu, L.C. Hsu, C.H. Ho, S.P. Liu, J.H. Guh, Phosphodiesterase type 5 inhibitors synergize vincristine in killing castration-resistant prostate cancer through amplifying mitotic arrest signaling, Front. Oncol. 10 (August) (2020) 1–14, https://doi.org/10.3389/fonc.2020.01274.